EDGE TURBULENCE AT PLASMA POLARISATION ON THE CASTOR TOKAMAK

M. HRON*, I. ĎURAN*, J. HORÁČEK*, K. JAKUBKA, L. KRYŠKA, J. STÖCKEL, F. ŽÁČEK

Institute of Plasma Physics, Acad. Sci. of the Czech Republic
P.O.Box 17, Prague 8, Czech Republic
**also: Faculty of Mathematics and Physics, Charles University, Prague, Czech Republic*

K. DYABILIN

High Energy Density Research Center, Inst. for High Temperatures, Moscow, Russia

S. NANOBASHVILI, I. NANOBASHVILI

Andronikashvili Institute of Physics, Tbilisi, Georgia

M. TENDLER

Royal Institute of Technology, Alfvén Laboratory, Stockholm, Sweden

G. VAN OOST

ERM/KMS, Laboratory for Plasma Physics, Brussels, Belgium

1 Introduction

Electrostatic turbulence is responsible for anomalous particle and heat losses from tokamak plasmas. The equilibrium level of plasma fluctuations is determined by competition of the growth rate γ and the damping rate ω of the most unstable modes.

The fluctuation growth rate is hardly to be deduced theoretically, namely at the plasma edge, where various models of the core and scrape-off layer turbulence overlap. A reasonable lower estimate of γ can be found from the autocorrelation time of fluctuations τ_A that can be easily derived from experimental data, $\gamma > 1/\tau_A$ [1].

On the other hand turbulence is damped by sheared plasma flows that are believed to be the main mechanism behind formation of transport barriers [2]. The plasma flows are closely related to the radial electric field, $E_r = \nabla p/(en) + v_p B_T + v_T B_p$. In the edge polarization experiments the radial electric field is mostly linked to the poloidal flow term $v_p B_T$ [5]. Consequently, damping of turbulent structures due to the sheared flow is characterised by the decorrelation rate $\omega_{E\times B} = dv_p/dr \approx (dE_r/dr)/B_T$. Reduction of the electrostatic turbulence can be expected if the $E \times B$ decorrelation rate prevails the growth rate γ. The described mechanism plays an essential role in the formation of edge [3] and internal [4] transport barriers as well as in tokamak regimes with edge plasma polarization (see e.g. [5],[6]).

The aim of this contribution is to study the impact of a sheared electric field on the spatial structure of edge fluctuations in the radial and poloidal directions on the CASTOR tokamak (R = 0.4 m, a = 0.085 m) [9]. A biased electrode is used for external modification of the radial electric field in the proximity of the natural velocity shear layer (VSL).

2 Experimental arrangement

Experiments have been carried out at B_T = 1 T, I_p = 8÷13 kA and line average densities $\bar{n}_e$ = 0.5÷1.5·10^{19}m^{-3}. The radial electric field is imposed to the edge plasma by a mushroom-like electrode biased with respect to the vacuum vessel by a voltage pulse. The fluctuations are monitored with the spatial resolution of 2.5 mm using two multiple Langmuir probes arrays, oriented in the radial and poloidal directions [9]. Individual tips measure either the floating potential U_{fl} or the ion saturation current I_{sat}.

All the key elements of the biasing experiments on the CASTOR tokamak are depicted in Fig. 1.

Fig. 1. Key elements of the biasing experiments: a) biasing electrode, mushroom-like shaped, made of carbon, with surface of 27 cm^2 (toroidally 80° from the limiter); b) radial probe array consists of 16 tips spaced by 2.5 mm, each tip is 2 mm long and 0.6 mm in diameter (220°); c) poloidal probe array has 18 tips, spaced also by 2.5 mm, the uninsulated part of each tip is again 2 mm (40°).

The specific feature of the analysed discharges is a downward shift of the plasma column, as schematically shown in Fig. 2.

The minor radius of the plasma column is already not determined by the radius of the poloidal limiter, but it is reduced to $a - \Delta$. As a consequence, an additional scrape-off layer appears. Its width is 2Δ at the top of the torus. The connection length in this region is much larger than the circumference of the torus ($2\pi R$) and varies with the safety factor $q(a - \Delta)$.

The radial electric field, which is one of the basic parameters of the biasing experiment, is deduced in a single shot using the radial probe array. The individual tips measure the floating potential, which is related to the plasma potential as $\Phi \cong U_{fl} + 2.5 \times kT_e/e$. The radial electric field is estimated as the gradient of the floating potential

$$E_r = -\nabla\Phi \cong -\nabla U_{fl} - 2.5 \times k\nabla T_e/e \approx -\nabla U_{fl} \,,$$

since the edge temperature profile is rather flat on the Castor tokamak ($k\nabla T_e/e \sim 0.1$ V/mm).

The vertical displacement of the plasma column is deduced from the vertical shift of the Velocity Shear Layer (VSL), defined here as the radius where ∇U_{fl} = 0. Simultaneous measurements of ∇U_{fl} and propagation velocity of fluctuations in the poloidal direction [7] show that

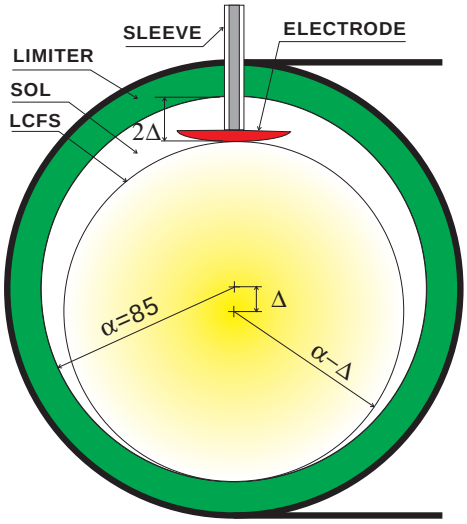

Fig. 2. Poloidal cross section, schematically showing the location of plasma column and biasing electrode.

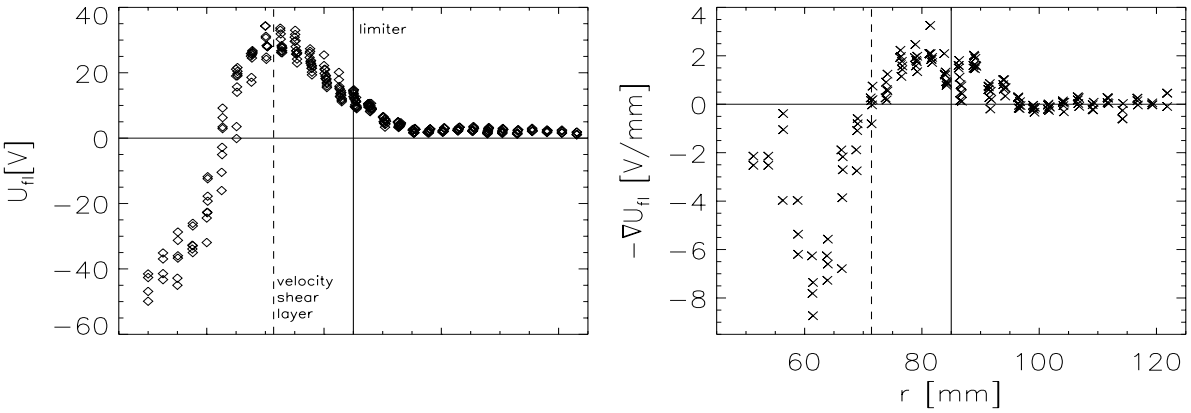

Fig. 3. a) Radial profile of the floating potential without biasing as measured by the radial probe array from the top of the torus. b) The gradient of the floating potential corresponds to the radial electric field: $E_r \approx -\nabla U_{fl}$.

the position of the real VSL is still a few millimeters more inside the plasma column (probably because the $\nabla T_e \neq 0$). However, in this contribution we refer the apparent position of VSL.

In the shot series shown here, the vertical displacement $\Delta = 6 \div 7$ mm.

Due to a strong poloidal asymmetry of the scrape-off layer, the probe arrays as well as the biasing electrode are located at the top of the torus, to define better their respective radial positions. The biasing electrode is radially located in the SOL, slightly outside the natural VSL. In fact, the electrode acts as a biased limiter. The aim of this configuration is to modify the shear of the radial electric field (defined as $\frac{dE_r}{dr}$) just in the proximity of the natural VSL by positive biasing. Another practical advantage of such configuration is that the radii $r < r_B$ are accessible by the probe arrays (r_B is the distance of the electrode from the center of the vacuum chamber).

3 Experimental results

3.1 Evolution of polarised discharges

The temporal evolution of a typical discharge with positive biasing is shown in Fig. 4. A voltage pulse is applied to the electrode during the quasistationary phase of the discharge. Typically, a current I_B = 30 ÷ 40 A is drawn by the electrode at U_B=+200 V. A fraction of the return current flows to the poloidal limiter ($\sim$ 30%), the remaining part flows directly to the vessel wall. The next panel shows the evolution of the intensity of the H_α spectral line I_{H_α}, which is proportional to the influx of neutral hydrogen atoms from the chamber wall. The small increase of I_{H_α}, observed at biasing, can not explain the significant increase of the line average density observed in the experiment. At the same time, the influx of impurities remains unchanged. Therefore, we conclude that the global particle confinement improves with biasing.

Quantitatively, the relative increase of the global particle confinement time τ_p^B/τ_p^{OH} can be estimated from the relation

$$\frac{\tau_p^B}{\tau_p^{OH}} \geq \frac{n^B}{n^{OH}} \frac{I_{H\alpha}^{OH}}{I_{H\alpha}^{B}}$$

The relative increase of τ_p by $\sim$ 50% is evident from the bottom panel.

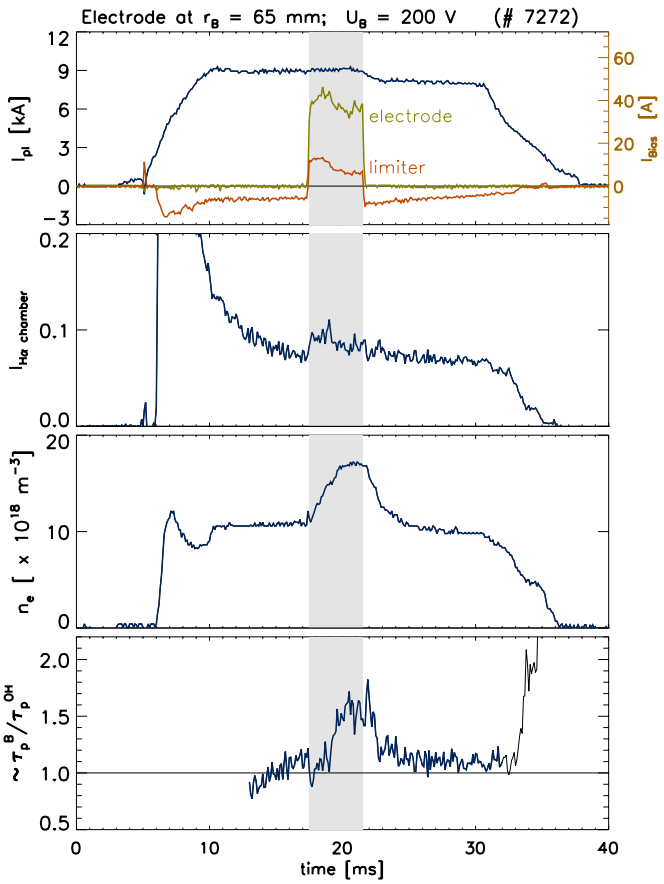

Fig. 4. Time evolution of some basic plasma parameters: a) plasma current (upper line, left y-axis), electrode current, and return current to the limiter (both right y-axis) b) Intensity of the H_α spectral line c) line average density $\bar{n}_e$ d) lower estimate of the relative increase of the particle confinement time.

When the biasing pulse terminates, the plasma density starts to decay exponentially to the original level as $n \sim e^{-t/\tau_N}$. The characteristic time $\tau_N \approx 1.4$ ms is a reliable estimate of the particle confinement time without biasing τ_p^{OH}.

These observations clearly indicate the formation of a transport barrier during the biasing period when the electrode is slightly outside the VSL.

It should be noted that even a stronger improvement of τ_p is observed, if the electrode is deeper immersed into the plasma, i.e. into the confinement region [8]. Moreover, in this case the H_α-line intensity drops with biasing by ~ 50 %. In contradiction with phenomena observed on the ISTTOK tokamak at limiter biasing experiments, the negative biasing on CASTOR shows only slight effect on the plasma confinement.

3.2 Radial profiles at the plasma edge

The response of the edge plasma to positive biasing is measured by the radial probe array. An example of the radial electric field measurements is shown in Fig. 5.

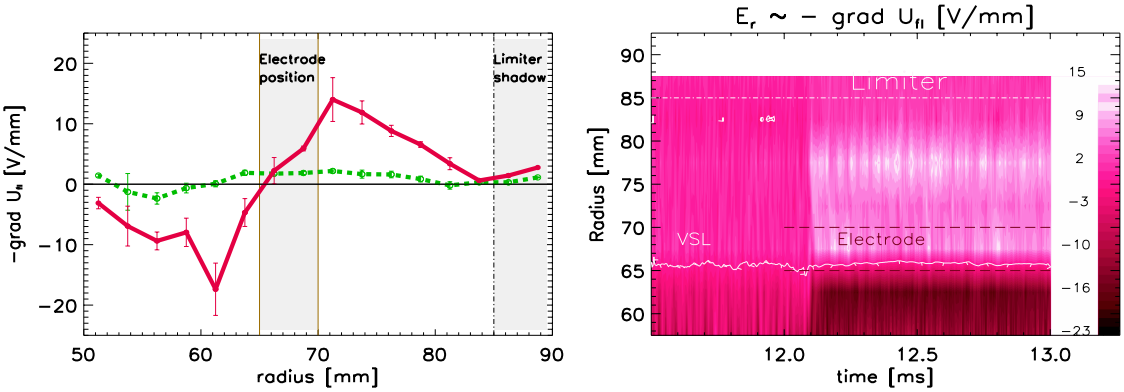

Fig. 5. Left: Radial profile of E_r without (dashed line) and with positive biasing + 200 V (solid line). Right: Gray scale plot of the spatial-temporal evolution of E_r; the scale (in V/mm) is indicated on the right hand side.

The left panel compares the time averaged profiles of the radial electric field without and with biasing. It is well seen that the electric field increases significantly with biasing at both sides of the VSL, i.e. in the SOL as well as in the edge plasma, reaching there values $\sim \pm$ 20 V/mm. The shear of the radial electric field increases from 0.8 up to 4 V/mm^2 at the separatrix.

The right panel shows an instantaneous radial profile of E_r, recorded in a single shot with the sampling 1 μs. The bright colours indicate regions with $E_r >$ +15 V/mm, while the dark regions correspond to the negative radial field ($E_r <$ -15 V/mm). The radial position of the VSL (marked by the white line) remains unchanged at biasing.

The increase of the E_r – shear strongly impacts the edge plasma density as demonstrated in Fig. 6. These plots are arranged in a similar way as the previous ones. The probe tips are operating in the ion saturation current mode. It is evident that the increase of the dE_r/dr is followed by a reduction of the edge density by a factor ~ 2 at $r < 65$ mm, i.e. inside the VSL. This, together with the increase of the line average density, indicates the formation of a steep density gradient somewhere deeper in the plasma column. Note also the reduction of density fluctuations in this region. One of the peculiarities of the biasing experiment is the increase of I_{sat} in the scrape-off layer.

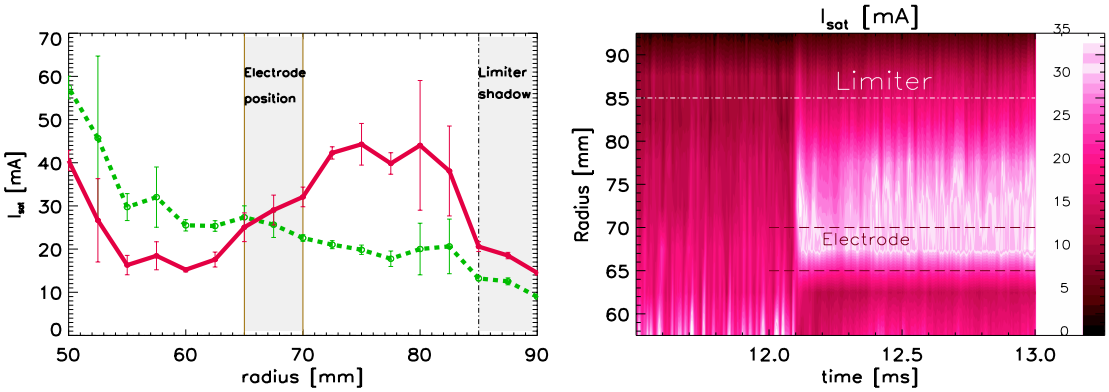

Fig. 6. Radial profile (left panel) and gray scale plot of the spatial-temporal evolution (right panel, #7355) of the ion saturation current.

The quasiperiodical structures ($f \sim 10$ kHz) in E_r and I_{sat} are formed in SOL during biasing as seen in Figs 5 and 6. They appear, when the biasing voltage exceeds $\sim$ +100 V. Similar "coherent" structures have been observed also on TEXTOR-94 [1], however, at higher frequencies.

3.3 Correlation analysis of fluctuations

The correlation analysis is used to deduce the characteristic dimensions/lifetimes of the turbulent structures and their propagation velocities [9].

The correlation length and phase velocity in the poloidal direction are deduced from correlation analysis of data from the poloidal probe array. The method and interpretation of results are described in [10]. The 2D plots of the spatial temporal correlation functions of the potential fluctuations are shown in Fig. 7 for nine shots differing in the radial position of the probe array.

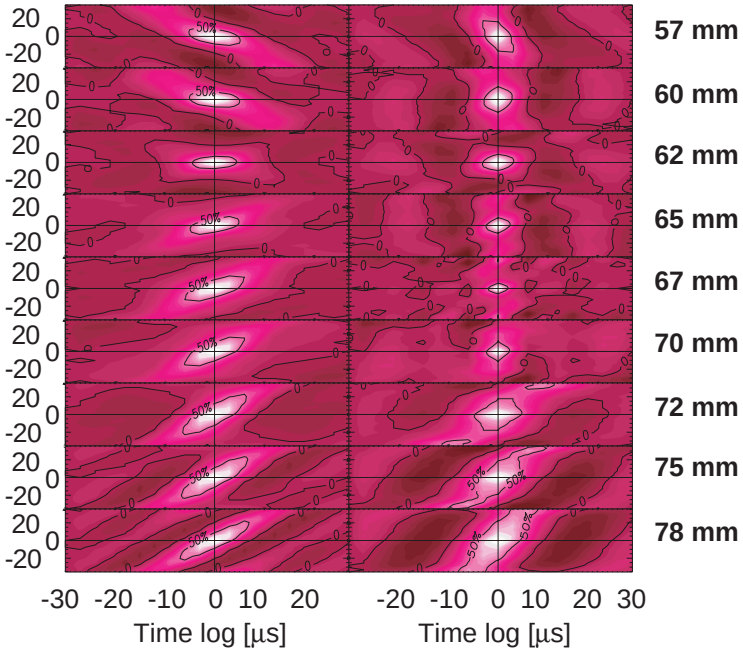

Fig. 7. Spatio-temporal correlation functions of the potential fluctuations for nine shots differing in the position of the poloidal probe array. The left (right) column corresponds to the situation without (with) biasing.

The horizontal axis of each panel is the time lag τ_{lag} (in μs), while the vertical axis represents the distance d_p along the probe array (in mm). The bright elliptical patterns correspond to combinations of τ_{lag} and d_p with a high correlation ($> 50\%$). The poloidal correlation length of turbulent structures is deduced here as the FWHM (Full Width at Half Maximum) of the correlation function at $\tau_{lag} = 0$. The sense and module of the poloidal velocity can be deduced from the slope of the correlation patterns.

Further, we compare here again the correlation patterns without (left column) and with (right column) biasing. It is well seen that, in the unpolarised plasma, the poloidal propagation reverses at the VSL, which is located at $r \sim 62$ mm in this shot series. During the polarised phase of the discharge, an increase of the propagation velocity is apparent outside as well as inside the VSL (compare the slopes of the correlation patterns with and without biasing at r = 57 mm and r = 75 mm). However, the form of correlation patterns in the region of the highest shear does not allow to determine neither the sense of propagation nor the module of poloidal velocity.

In the radial direction, the turbulent structures are characterised by computing the correlation coefficient $C_{i,j}$ ($i, j = 1 \div 16$) between the signals of the tips of the radial probe array. The time lag was taken as zero. Examples of the resulting radial profiles of $C_{i,j}$ are shown in Fig. 8.

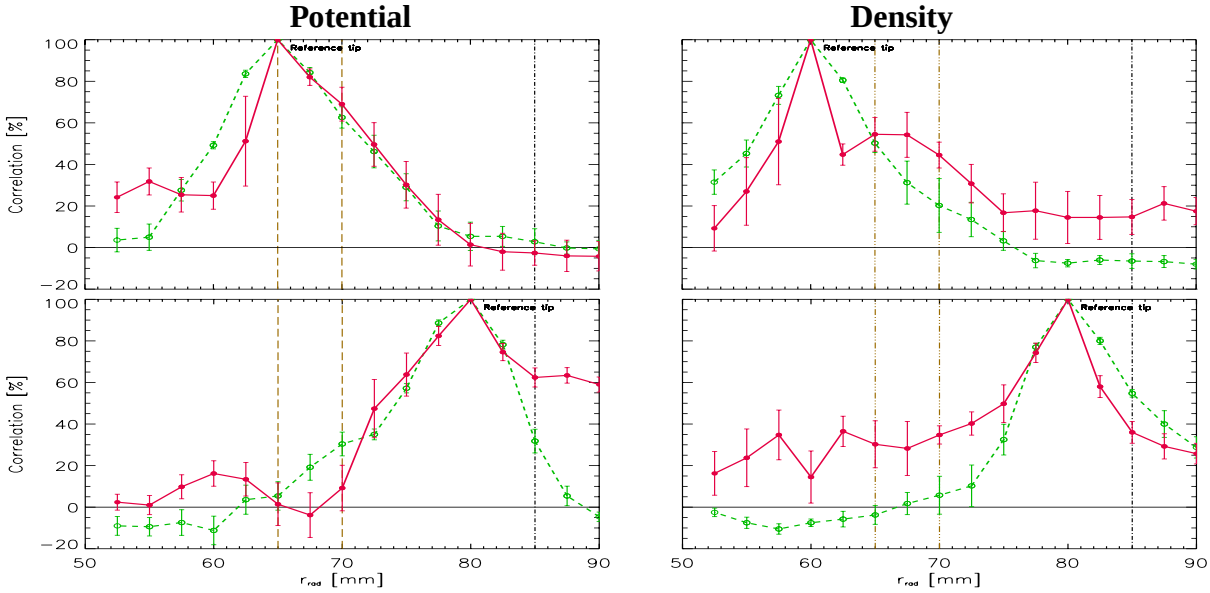

Fig. 8. Spatial correlation of the potential (left column) and density (right column) fluctuations in the radial direction. Correlations without (dashed line) and with (solid line) biasing are compared. First row: the reference tip is in the proximity of the VSL; Second row: the reference tip is in the SOL.

We see that the spatial cross-correlation functions without biasing (dashed green lines) appear to be symmetric around the position of the reference tip independently, whether the tip is in the proximity of the VSL or elsewhere. The radial correlation length, deduced here as the half width of the cross-correlation function is of about 10 mm. On the other hand, with biasing, the spatial correlation function is strongly asymmetric, namely if the reference tip is in proximity of the VSL (see the first row in Fig. 8). This is because the radial correlation length is already comparable or even shorter than the distance between the tips. To overcome this problem, the

correlation coefficients $C_{i,i+1}$ of signals of the adjacent tips are taken as a measure of the radial correlation length in polarised discharges.

The resulting radial profiles of the quantities which characterise the turbulent structures in the radial and poloidal directions are plotted in Fig. 9.

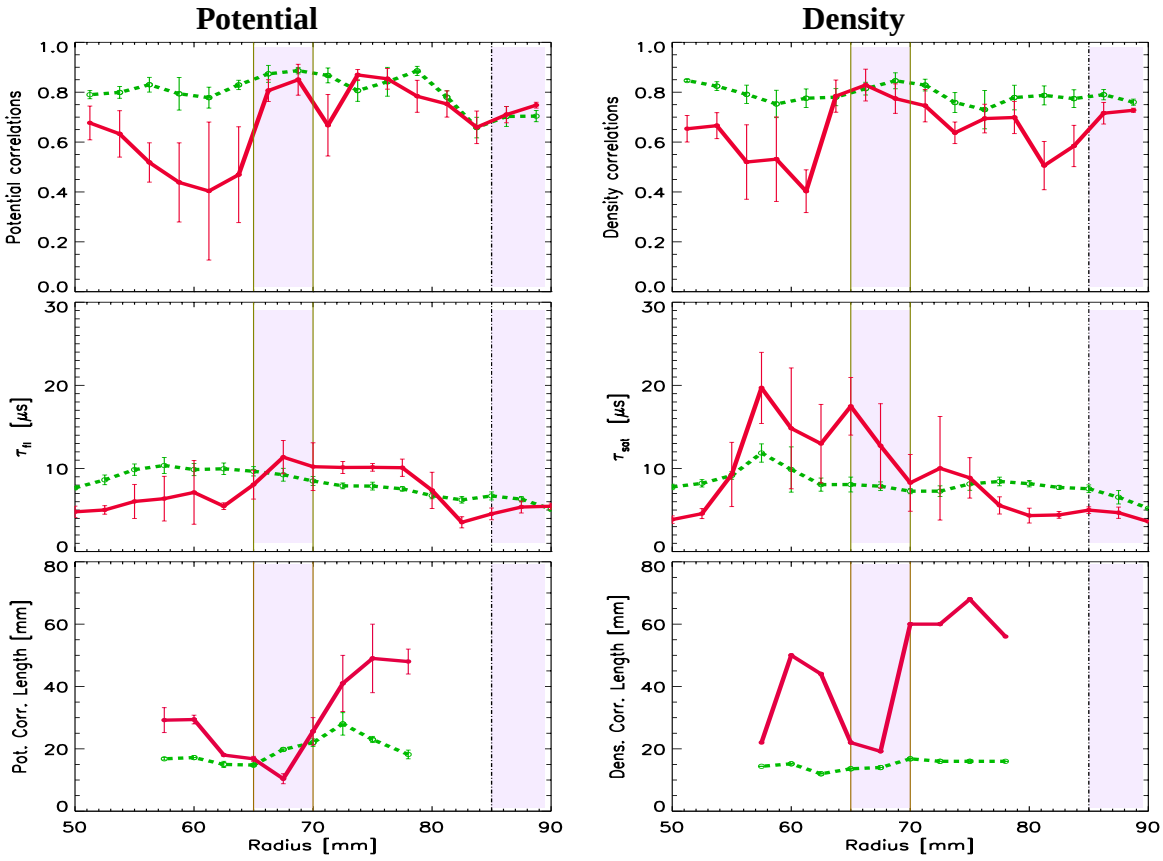

Fig. 9. Radial profiles of the parameters, characterising the potential (left column) and density (right column) fluctuations without (dashed lines) and with (solid lines) positive biasing. The positions of the electrode and of the poloidal limiter are marked by shadowing. The profiles shown in the first two rows are derived using the radial probe array, while the last row corresponds to data from the poloidal probe array measured on the shot-to-shot basis. Individual rows (from top to bottom): Correlation coefficient $C_{i,i+1}$ of signals of adjacent tips (proportional to the radial correlation length), the autocorrelation time (determined as the FWHM of the autocorrelation function) and the poloidal correlation length.

As it is evident from this figure, the enhancement of the E_r - shear by a factor of ~ 5 at biasing is followed by a complex response of the edge turbulence. A dramatic drop of the potential as well as of the density correlation coefficients $C_{i,i+1}$ are observed in the region, where E_r appears to be more negative, i.e. in the confinement region. On the other hand, fluctuations seem to be radially "untouched" within the scrape-off layer ($E_r > 0$). One should note that the drop of $C_{i,i+1}$ below 0.5 implies a reduction of the radial correlation length below 2.5 mm.

The reduction of the autocorrelation time, observed at $E_r < 0$ for potential fluctuation and at $E_r > 0$ for the density fluctuation can be explained either by a reduction of the life time of the fluctuations or by a Doppler shift, which appears due to an enhanced poloidal rotation. On the other hand, an increase of τ_A (observed in SOL for the potential fluctuations and in the edge

plasma for the density fluctuations) can be attributed only to an increase of average lifetime of turbulent structures.

The poloidal correlation length is reduced or remains unchanged only at radii corresponding to the radial position of the biasing electrode. However, it increases significantly with biasing at both sides of the electrode.

3.4 Fluctuation-induced flux in polarised plasmas

The fluctuation-induced flux Γ, which is generally believed to be responsible for particle losses from tokamak plasmas [11], is determined by the cross-correlation of the density δn and poloidal electric field fluctuations δE_p as

$$\Gamma = < \delta n \delta E_p > / B_T \tag{1}$$

Alternatively, Γ can be expressed as a product of the rms values of the density ($\tilde{n} = \sqrt{< \delta n^2 >}$) and of the poloidal electric field ($\tilde{E}_p = \sqrt{< \delta E_p^2 >}$) fluctuations

$$\Gamma = (\tilde{n} \tilde{E}_p \cos\alpha)/B_T \quad , \tag{2}$$

where α is the phase angle between the density and E_p fluctuations [1].

The flux Γ can be easily experimentally deduced using the poloidal probe array operating with odd tips in the floating mode and even tips in the ion saturation current mode [10]. The radial profiles of Γ without (green dashed line) and with (red solid line) biasing are compared in Fig. 10.

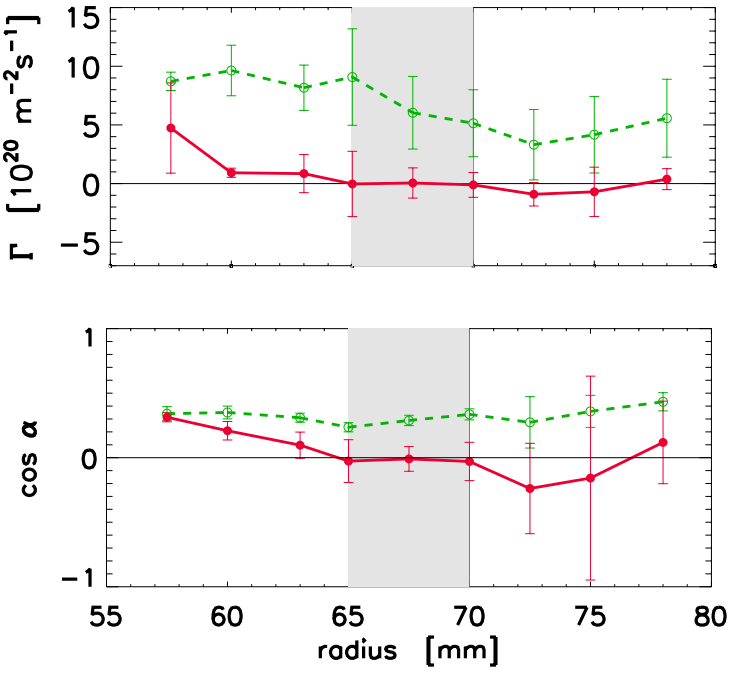

Fig. 10. Fluctuation-induced flux Γ and the phase angle between the density and poloidal electric field fluctuations, $\cos\alpha = < \delta n \delta E_p > / \sqrt{< \delta n^2 >< \delta E_p^2 >}$.

As seen, the fluctuation-induced flux is practically suppressed outside the VSL. At the same time, the levels of n and E_p fluctuations are only slightly reduced. Therefore, the suppression of Γ is mainly due to the increase of the phase between the density and poloidal field fluctuations. Similar observation was reported in [1].

4 Conclusions

Experiments on the Castor tokamak demonstrate the possibility to form a transport barrier in the edge plasma using a massive graphite electrode, positioned in the scrape of layer and biased at +200 V. The radial electric field is affected not only between the electrode and the vacuum vessel as expected but also by the formation of a negative field of the same order of magnitude within the last closed flux surface. The global particle confinement improves by $\sim 50\%$.

The resulting shear of the radial electric field in the separatrix region is as high as 4 V/mm^2 which reveals the $E \times B$ decorrelation rate $\omega_{E\times B} \sim 4 \times 10^6$ s^{-1}. This value is essentially higher than the expected growth rate of the edge electrostatic fluctuations $\gamma \sim 10^5 \div 10^6$ s^{-1}.

The enhanced shear of the radial electric field in the separatrix region in polarised discharges impacts dramatically on the edge electrostatic fluctuations as shown by the spatial-temporal resolved probe measurements. Some observed features, such as the radial decorrelation in the proximity of VSL, can be expected. However, the observed increase of the poloidal correlation and lifetime of fluctuations is not understood up to now. The last effect could be related to a quasiperiodic low frequency component ($f \leq 10$ kHz) of the plasma fluctuations, which appears when dE_r/dr prevails a critical value. Such modulation is even more apparent, if the electrode is deeper immersed in the edge plasma and biased to more than +150 V.

In conclusion, we show in this contribution that the polarization of the edge plasma, if it is accompanied with the spatially resolved measurement of the plasma fluctuations, represents an useful experimental tool to control the ExB decorrelation of the turbulent structures in the edge plasma of tokamaks. It is evident, however, that the correct interpretation of the complex behaviour of the edge turbulence shown here requires additional experiments.

Supported by the grant A1043701 of the Czech Academy of Sciences.

References

[1] J. Boedo, G. Van Oost *et al.*: Czech. J. Phys. **48**, Suppl. S3 (1998) 99.
[2] M. Tendler: Plasma Phys. Control. Fusion **39** (1997) B371-B382.
[3] F. Wagner *et al.*: Phys. Rev. Lett. **49** (1982) 1408.
[4] E.J. Synakowski *et al.*: Phys. Plasmas **4**(5) (1997) 1736.
[5] R.R. Weynants *et al.*: Plasma Phys. Contr. Fusion **40** (1998) 634.
[6] J.A.C. Cabral *et al.*: Plasma Phys. Control. Fusion **40** (1998) 1001-1019.
[7] For more details, see http://www.ipp.cas.cz/tokamak/castor/recent.htm
[8] F. Žáček *et al.*: Czech. J. Phys. **48**, Suppl. S3 (1998) 60.
[9] J. Stöckel *et al.*: Plasma Phys. Control. Fusion **41** (1999) A577-A585.
[10] J. Petržílka, J. Stöckel: Contrib. Plasma Phys. **38S** (1998) 74.
[11] M. Endler *et al.*: Nucl. Fusion **35** (1995) 1307.